AGU PUBLICATIONS

JGR

Journal of Geophysical Research: Oceans

RESEARCH ARTICLE

10.1002/2015JC011354

Key Points:
- Surface circulation at the Strait of Gibraltar
- HF radar and model intercomparison
- Operational observatory system

Correspondence to:
P. Lorente,
plorente@puertos.es

Citation:
Soto-Navarro, J., P. Lorente, E. Álvarez Fanjul, J. Carlos Sánchez-Garrido, and J. García-Lafuente (2016), Surface circulation at the Strait of Gibraltar: A combined HF radar and high resolution model study, *J. Geophys. Res. Oceans*, *121*, doi:10.1002/2015JC011354.

Received 29 SEP 2015
Accepted 26 FEB 2016
Accepted article online 1 MAR 2016

Surface circulation at the Strait of Gibraltar: A combined HF radar and high resolution model study

Javier Soto-Navarro[1], Pablo Lorente[1], Enrique Álvarez Fanjul[1], Jose Carlos Sánchez-Garrido[2], and Jesús García-Lafuente[2]

[1]Área de Medio Físico, Puertos del Estado, Madrid, Spain, [2]Physical Oceanography Group of the University of Málaga (GOFIMA), Málaga, Spain

Abstract Observations from a high frequency radar system and outputs from a high resolution operational ocean model working at the Strait of Gibraltar have been analyzed and compared during the period February 2013 to September 2014 in order to evaluate their capability to resolve the surface circulation of the region. The description of the mean circulation patterns has been statistically assessed, showing good agreement, particularly in the central region of the strait corresponding with the Atlantic Jet (AJ) stream, although some short scale features are not reproduced by the model. In the frequency domain very high concordance is observed. Tidal maps of diurnal and semidiurnal constituents are in good agreement with previous observations. The analysis of the model and radar response to the wind forcing reveals that the low resolution of the model wind-forcing field and its deeper superficial level smoothes the wind effect on the simulated currents. The first three EOF modes account for the 86% of model and radar variances. The coincidence between the observed and simulated patterns is very significant for the first two modes, which account for the mean velocity field and the latitudinal shifting of the AJ consequence of the flow-topography interaction. The third mode captures the wind-induced circulation, and greater discrepancies are found in this case. Results underline the complementary character of both systems: radar observations improve the model description, resolving short scale processes, while the model completes the radar information when the time or spatial coverage is poorer.

1. Introduction

As the only connection between the Atlantic Ocean and the Mediterranean Sea, the Strait of Gibraltar is a key spot from the geostrategic and scientific standpoints. Its topography is characterized by a rather complicated system of sills and narrows which extends nearly 60 km, with a mean width of 20 km. The minimum depth, of less than 300 m is located at Camarinal Sill (CS in Figure 1), and the minimum width, of around 14 km, is found at the Tarifa Narrow (TN in Figure 1).

The freshwater deficit over the Mediterranean basin, consequence of the excess of evaporation over precipitation and river runoff, drives a two-layer baroclinic exchange [*Bethoux and Gentilli*, 1999; *Mariotti et al*., 2002; *Criado-Aldeanueva et al*., 2012]: a relatively fresh and warm time-averaged Atlantic inflow of 0.81 ± 0.06 Sv (1 Sv $= 10^6$ m^3/s) enters the basin flowing eastward in the upper layer while a cooler and saltier Mediterranean outflow of -0.78 ± 0.05 Sv leaves the strait flowing westward in the lower layer, resulting in a net flow of 0.038 ± 0.007 Sv [*Soto-Navarro et al*., 2010].

The exchange is not steady but highly variable at different time scales. Low frequency seasonal and interannual variability are mainly driven by the climatic forcing over the Mediterranean basin [*García-Lafuente et al*., 2002a, 2009]. In the subinertial band (O (10 days)), the changes in the atmospheric pressure over the Western Mediterranean are the main mechanism affecting the flow, although the wind stress over the Atlantic side of the Strait also plays some role [*Candela et al*., 1989; *García-Lafuente et al*., 2002b]. By far, the diurnal and semidiurnal tides are the most important source of transport variability, which causes the mean flow of the upper or lower layer to reverse in almost every tidal cycle at different locations along the Strait. For instance, the tidal transport associated with M_2 and S_2 constituents reaches values as high as 4 Sv [*García-Lafuente et al*., 2000; *Sánchez-Román et al*., 2012]. Although the meteorological wind forcing effect is rather restricted to the superficial layer, it might also be a key factor in specific processes such as punctual

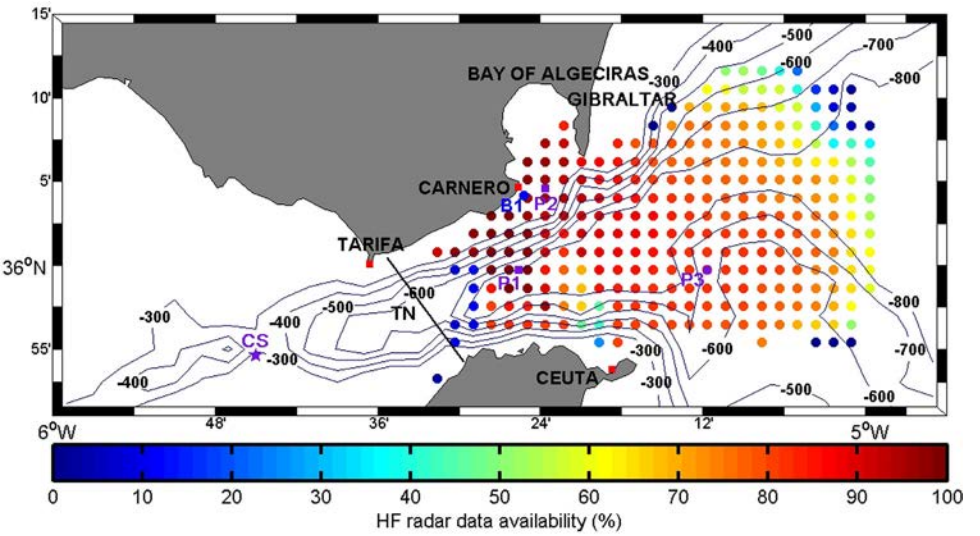

Figure 1. Bathymetric map of the Strait of Gibraltar. Points delimitate the HFR domain and the color scale represents the time coverage in % for the studied period (February 2013 to September 2014). Note that only one every two points is represented for clarity reasons. Red squares indicate the position of the radar sites (Tarifa, Punta Carnero and Ceuta). P1, P2 and P3 are the points whose time series of the zonal and meridional components are analyzed in section 3.1. B1 denote the position of the Punta Carnero buoy, CS the location of Camarinal Sill and TN the location of Tarifa Narrow.

inflow interruptions [*García-Lafuente et al*., 2002c] or the circulation pattern in the Bay of Algeciras [*Sánchez-Garrido et al*., 2014].

Concerning human activities, in addition of being the gate to the Mediterranean, the presence of the important harbors of Algeciras and Gibraltar (Figure 1) concentrates one of the most intense maritime traffics in the world, with more than 100,000 ships sailing through this relatively small region every year. This supposes the circulation of more than 20 million tons of fuel, with the subsequent potential risk of oil spill accidents, not only harmful for the remarkable ecology of the region, but more importantly for the tourism-based economy of the surrounding cities. Moreover, the high activity in the area entails an important number of search and rescue operations. For instance, only in year 2013, 492 emergencies were addressed, involving 3869 people (data from the Salvanto Marítimo, the Spanish search and rescue agency).

The previous considerations underline the necessity of an efficient current monitoring in the area. For this purpose two complementary systems are currently working at the Strait: a high resolution numerical model, developed as part of an operational oceanography system in the frame of the Sistema Autonomo de Medicion, Prediccion y Alerta en la Bahia de Algeciras (SAMPA) project, which is shortly described in section 2.2, and a High Frequency Radar (HFR) system deployed as part of the European funded Transnational RADars for Environmental applications (TRADE) project.

The reliability of HFR measurements, which are affected by intrinsic uncertainties like spurious signals from radio frequency interferences, antenna pattern distortions or environmental noise [*Kohut and Glenn*, 2003], has been previously tested in a number of validation studies. Such studies include comparisons of HFR-derived surface currents with moored Acoustic Doppler Current Profilers (ADCP) [*Chapman et al*., 1997; *Kaplan et al*., 2005; *Cosoli et al*., 2010], point-wise current meters [*Graber et al*., 1997; *Emery et al*., 2004; *Paduan et al*., 2006] or drifters [*Ohlmann et al*., 2007; *Molcard et al*., 2009; *Shadden et al*., 2009]. In this context, previous validation works have been performed with the Gibraltar HFR system in order to assess the accuracy of both radial and total current vectors [*Lorente et al*., 2014] as an extension of previous validation works achieved with the growing HFR network operated by Puertos del Estado [*Alfonso et al*., 2006; *Lorente et al*., 2015]. SAMPA model outputs have been validated using ADCP and Conductivity-Temperature (CT) probes data from a set of moorings at different locations in the Strait area [*Sánchez-Garrido et al*., 2013; *Sammartino et al*., 2014] and satellite Sea Surface Temperature (SST). Both systems have proven to properly represent the dynamic of the Strait area.

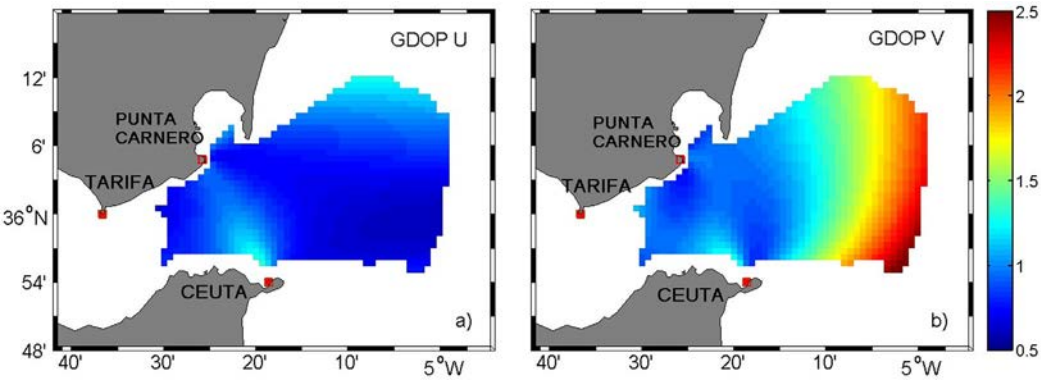

Figure 2. Geometric Dilution Of Precision (GDOP) of the Strait of Gibraltar HFR system for the (a) zonal and (b) meridional components.

The advantages of using HFR measurements for the evaluation of regional circulation models have been also analyzed by several authors [*Chavanne et al*., 2007; *Mau et al*., 2007; *Cosoli et al*., 2013; O'*Donncha et al*., 2015], revealing that models and HFR work as complementary systems. Following this line, the present study aims at assessing the skills of the two systems operating at the Strait of Gibraltar to resolve the surface circulation of the region by means of detailed statistical and qualitative comparison of their performance, and to understand how they complement to each other. The data sets and methodology applied are described in section 2, and the results are exposed and discussed in section 3. Finally a summary and the concluding remarks are presented in section 4.

2. Data and Methods

2.1. HF Radar Data

The HFR technology, based on the principle of Bragg scattering of the electromagnetic radiation over a rough sea [*Crombie*, 1955], infer the radial current component from the Doppler-shift of radio waves backscattered by surface gravity waves of half their electromagnetic wavelength. Each single radar station or site can estimate radial currents moving toward or away from it out to distances as far as dozens of kilometers. In regions of overlapping coverage from two or more stations, a least squares fitting technique is used to compute the zonal and meridional components of the horizontal current [*Lipa and Barrick*, 1983].

The CODAR SeaSonde HF radars used in this study were deployed in 2011 at the Strait of Gibraltar (Figure 1) in order to monitor, in near real time, the surface current field in this geostrategic region efficiently. It consists of three shore-based short-range sites deployed in two different stages: the first two stations became operative in May 2011 (Ceuta, 39.90°N 5.31°W, and Punta Carnero, 36.08°N 5.43°W, see Figure 1) whereas the third station (Tarifa, 36°N 5.61°W) was added to the existing network in October 2012.

Each site is operating at a central frequency of 26.8 MHz with a 150 KHz bandwidth, providing hourly radial measurements with a cut-off filter of 250 $cm \cdot s^{-1}$, a threshold that has been established according to the historical values observed in the area. The maximum horizontal range is set to 40 km and the HFR angular resolution is 5°. The estimated current velocities are representative of the upper 0.5 m of the water column. Only calibrated (measured) antenna patterns are used to process radial data [*Lipa et al*., 2006]. Radial current measurements from the three stations are geometrically combined with an averaging radius set to 3 km, in order to estimate hourly total current vectors on a Cartesian regular grid of 1x1 km horizontal resolution. The system covers the easternmost area of the Strait, including the mouth of the Bay of Algeciras, and part of the western Alboran Sea (Figure 1).

A source of error to be considered in the computation of the total vectors is the Geometrical Dilution Of Precision (GDOP). The GDOP is defined as a dimensionless coefficient of uncertainty that characterizes the effect of the geometry of the coupled radar sites on the measurements accuracy and position determination errors [*Levanon*, 2000; *Trujillo et al*., 2004]. In the region close to the baseline (the line joining two HFR stations) the radial vectors are almost parallel so the GDOP increases in such a way that the system accuracy to produce total vectors decreases. To reduce this problem, an interpolation procedure is carried out, filling

the gaps of the domain in the areas close to the baselines where the GDOP is very high [*CODAR Ocean Sensors, Ltd*., 2004]. The same problem appears in some of the outer regions of the domain, where the large distance to the stations makes the radial vectors to be nearly parallel too.

The Figure 2 illustrates the zonal and meridional components of the GDOP over the HFR domain, estimated according to the formulation of *Barrick* [2006]. The values of GDOP in the baselines are low, less than 1.2 for both components. This is the result of using radial vectors from the three stations in the computation of the total velocities, one of the main reasons to deploy the Tarifa station in the second stage of the TRADE project. The spatial distribution of the stations allows resolving the central region of the Strait, minimizing the GDOP of the system in this sensitive area. The baseline between Ceuta and Punta Carnero stations is resolved using radial vectors from the Tarifa station, while the baseline between Tarifa and Ceuta stations is resolved using the vectors from Punta Carnero. On the other hand, the GDOP for the meridional component increases in the eastern region of the domain, reaching values of 2.5 in the boundary (Figure 2b). In this area only radial vectors from Punta Carnero and Ceuta are used to compute the total velocities and the direction of their radial vectors is almost parallel.

In order to assess the accuracy of the HFR system, *Lorente et al*. [2014] compared radial and total current vectors with direct current measurements from Punta Carnero coastal buoy (B1 in Figure 1) during a 47 day period (19 October to 4 December 2013). Although the location of B1, close to the coast and the radar site, is not optimal for the comparison, the results for the radial vectors showed root mean square errors (8–22 $cm{\cdot}s^{-1}$), angular offsets (2°–30°) and correlations (0.31–0.81) in the range of previous studies using the same methodology [*Emery et al*., 2004; *Paduan et al*., 2006; *Cosoli et al*., 2010]. Higher discrepancies were observed for the Tarifa station, whose position with respect to B1 made the results inaccurate because the line joining the station and the buoy is very close to the land where the radial vectors are strongly affected by interferences. For the zonal and meridional components of the total vectors the results are also satisfactory, with correlations of 0.77 and 0.47 respectively, in the range of those obtained in previous works [*Kaplan et al*., 2005; *Cosoli et al*., 2010]. The higher discrepancies observed for the meridional component are ascribed to the stronger variance in the HFR measurements. *Lorente et al*. [2014] also show that the Gibraltar HFR system properly represents the basic oceanographic features and well-known mean circulation patterns observed in the area of study.

HFR data from February 2013 to September 2014 have been used in this study. As shown in figure 1, data availability is higher than 75% in most of the domain for this period, decreasing in the northeastern section. The mean velocity field provided by the system captures the main features of the area, i.e., the Atlantic Jet (AJ) and a small portion of the WAG, whose interaction generates a rather complicated circulation pattern.

2.2. Numerical Model

The model used in this work is a regional implementation of the Massachusetts Institute of Technology global circulation model (MITgcm) [*Marshall et al*., 1997]. The setup is similar to that described in detail by *Sánchez-Garrido et al*. [2013] and *Sammartino et al*. [2014]. The domain extends from the Gulf of Cádiz to the Alboran Sea (from 9°W to 1°E), and has been discretized with an orthonormal curvilinear grid of variable horizontal resolution (sparser close to the boundaries, $\sim$ 8–10 km, and higher in the Strait area, where Δx, $\Delta y \sim$ 300–500 m). In the vertical, it has 46 unevenly spaced z-levels with maximum resolution of 5 m near the surface, exponentially decaying toward the seafloor. The shallower level is at 2.5 m depth. The bottom topography is represented as partial vertical cells.

In the lateral boundaries the model is forced by daily mean temperature, salinity and velocity fields from the MyOcean Med large scale circulation model [*Oddo et al*., 2009]. In addition, tidal and meteorologically driven barotropic velocities are prescribed across the open boundaries, the former extracted from the model described by *Carrere and Lyard* [2003] and the latter from the storm surge operational system developed by *Álvarez-Fanjul et al*. [2001], which accounts for the remote effect of the atmospheric forcing in the barotropic flow through the strait. At the sea surface, the model is forced by 3 hourly values of wind stress, fresh water and heat surface fluxes provided by the Spanish Meteorological Agency through the operational Forecast System based on the HIRLAM model [*Cats and Wolters*, 1996]. A comprehensive description of the model parameterization can be found in the above mentioned references.

The SAMPA model has been extensively validated using velocity profiles from ADCP and salinity and temperature records from CT sensors. During spring 2011 *Sammartino et al*. [2014] carried out a validation campaign using five moorings deployed in the Bay of Algeciras. The authors found very good agreement between model outputs and observations, with correlations (at 95% confidence level) ranging between 0.80 and 0.95 for temperature and between 0.78 and 0.83 for salinity. The observed and modeled amplitudes for the M_2 tidal constituent showed differences of less than 10% ($\sim$ 3 cm) in all the moorings and the phase errors were lower than 4.4°. The S_2 modeled and observed amplitudes coincided within the confidence intervals and the difference of phases were lower than 5°. These authors also demonstrate the model capability to describe the tidal flows and the internal circulation of the bay. *Sánchez-Garrido et al*. [2014], using complementary observations collected in autumn 2011, showed that the model is also able to properly reproduce the ventilation mechanisms and flushing times of the Bay.

Using satellite SST images for autumn 2011 over the complete domain, *Sánchez-Garrido et al*. [2013] studied the formation and collapse of the Western Alboran Gyre, showing that the SAMPA model is able to reproduce this process thus helping to understand the complex processes that triggered the event. For integrated variables such as the Mediterranean outflow, these authors found a difference of less than 10% between the model and observations-based estimations of the flow leaving the Strait through the westernmost gateway of Espartel sill.

The model data used in this study cover the same period as the HFR data (February 2013 to September 2014), except for a gap of 27 days in May 2013 when the model outputs were lost due to a technical failure in the storage system and the data could not be recovered or reproduced.

2.3. Punta Carnero Buoy Wind Data

The original wind record, collected at 3 m height by the WatchKeeper buoy of Puertos del Estado moored at Punta Carnero (36.07°N 5.42°W, 40 m depth; B1 in Figure 1) has been filtered using a 12 order low-pass Butterworth function with a cutoff period of 30h, and the zonal component of wind stress (τ_x) has been computed following the formulation of *Large and Pond* [1981]. On the other hand, the hourly values of wind velocity have been used to identify periods of easterlies and westerlies, the two prevailing winds in the area [*Dorman et al*., 1995], in order to assess the performance of the wind-induced circulation predicted by the HFR system and by the SAMPA model. Finally, the periods from 5 to 9 November 2013 and 26 to 30 November 2013 have been selected as representatives of westerlies and easterlies, respectively.

2.4. Data Analysis

Model data were bilinearly interpolated into the sparser radar grid so that the analysis could be performed in the same domain and domain grid. Radar and model time series of the zonal and meridional velocity components at three different locations have been analyzed, estimating correlations and current roses. The statistical comparison between HFR and SAMPA velocity fields has been carried out by means of the variance, complex correlation and veering angle [*Kundu*, 1976]. Scalar correlation and root mean square error (RMSE) for the zonal and meridional components have also been calculated. All the metrics are estimated at 95% significance level, which has been computed using the Student's *t* test.

For each grid point, data gaps shorter than 24h were previously interpolated using a function that accounts for the main variability of periods shorter than a day, i.e., tidal (M_2 and S_2) and inertial (20.4h period at 36°N) fluctuations [*Chavanne et al*., 2007]. Sinusoids with M_2, S_2 and inertial frequencies were least square fitted to the available observations in a 6 day window centered on each missing data segment. A linear trend was also added to match the interpolation with the observations in the edges of each segment. Only grid points with more than 75% time coverage were used. The dominant frequency components were estimated computing the rotary autoespectra for both SAMPA and HFR data. Smooth estimates of the spectral energy were obtained applying the modified-periodogram approach, using 512h data segments with 50% overlap and a Hamming window [*Welch*, 1967]. Finally, the obtained spectral densities at each grid point were spatially averaged. Due to malfunctions of Punta Carnero buoy, only data between 12 May 2013 and 31 December 2013 are suitable for this computation.

The harmonic analysis of the velocity data was performed using the t_tide Matlab package [*Pawlowicz et al*., 2002]. Major and minor axis, inclination and phase of the tide ellipses for the main semidiurnal (M_2 and S_2) and diurnal (K_1 and O_1) constituents were estimated and analyzed at each grid point. Sea breezes are not

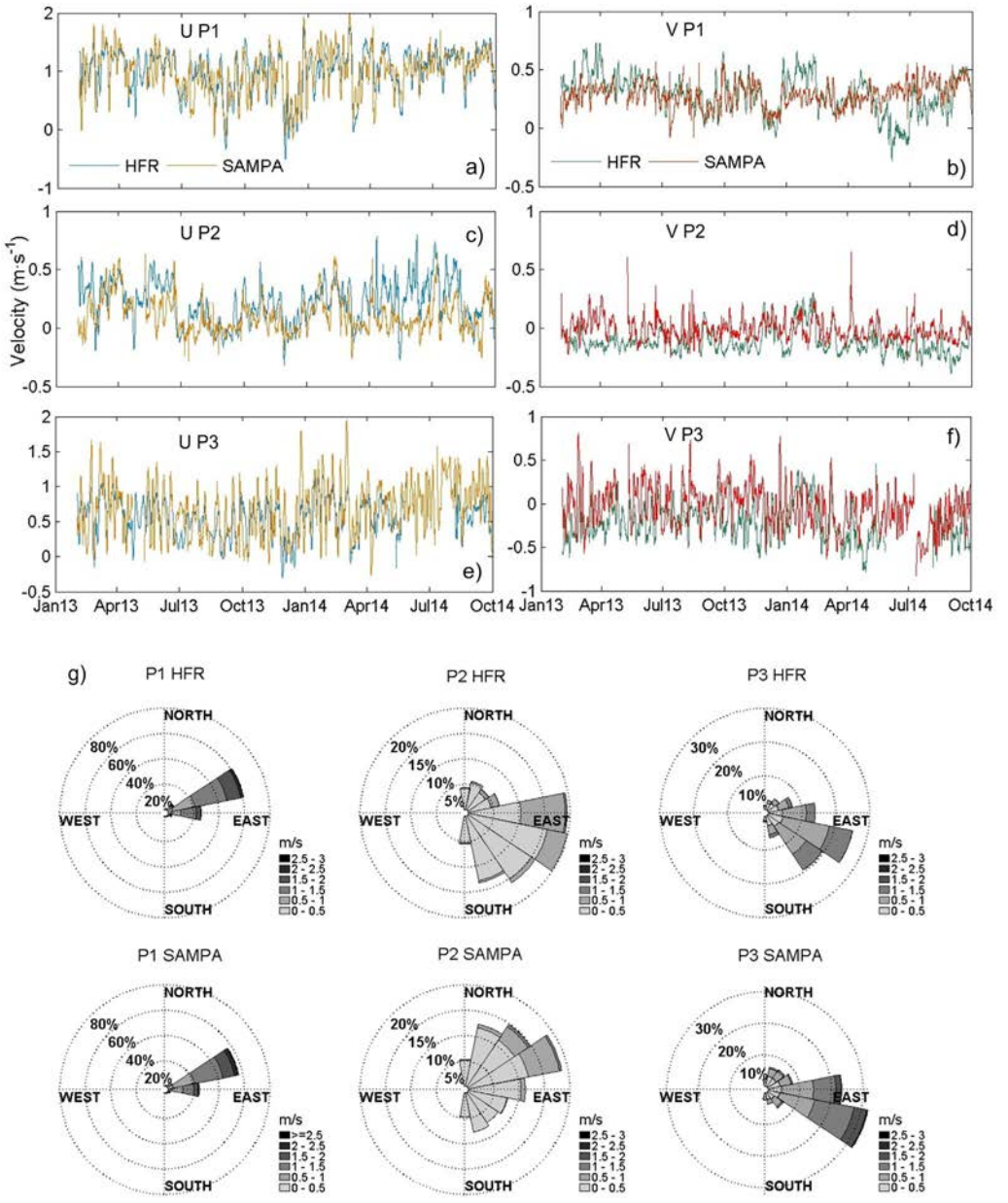

Figure 3. A 30 h running mean series of the HFR and SAMPA (left) zonal and (right) meridional components of the velocity at points (a, b) P1, (c, d) P2, and (d, f) P3. (g) The roses of current at the same points.

expected to influence the harmonic constants of the diurnal constituents because the length of the time series used in the analysis is longer than a year.

In order to explain and compare the skills of radar and model to resolve the patterns that dominate the spatial variability of the Strait, real valued empirical orthogonal function (EOF) decomposition [*Kaihatu et al.*, 1998] was performed to the original time series. The EOF modes were computed after applying the same interpolation described for the estimation of the rotary spectra, and hence for the same subset of data.

3. Results and Discussion

3.1. Time Series Analysis

As a first step in the comparison between HFR and SAMPA systems, time series of the velocity components at three different locations of the domain (P1, P2 and P3 in Figure 1) have been extracted and analyzed. P1

Table 1. Correlation at 95% Confident Level Between HFR and SAMPA Zonal and Meridional Velocity Components at the Three Points Analyzed (See Text, Figure 1)[a]

	P1		P2		P3	
	U	V	U	V	U	V
Raw correlation	0.70	0.27	0.41	0.22	0.54	0.29
30 h running-mean correlation	0.77	0.32	0.52	0.35	0.63	0.30

[a]First row correspond to the hourly time series and second row to the 30h running-mean filtered time series represented in Figure 2.

is located in the center of the Strait and P3 in the eastern region, both in the path of the AJ. P2 is close to the coast, at the mouth of the Bay of Algeciras, and it lies off the AJ main pathway. Due to its proximity to the Punta Carnero site, this point is likely affected by GDOP. Although the interpolation process described in section 2.1 for the points close to the baselines is applied here, this particularity must be taken into account in the interpretation of the results. Despite this, P2 has been pointedly selected for two reasons: on one hand, to compare HFR and SAMPA outside of the main AJ pathway, where the zonal and meridional components of the velocity are comparable and, on the other hand, to evaluate the HFR and SAMPA performance at the mouth of the Bay of Algeciras, a sensitive point in the Strait area.

Figure 3 shows the 30h running mean time series and the current roses for each point. For P1 and P3 a very good agreement is observed for the zonal component (Figures 3a and 3e), with correlations of 0.70 and 0.54 respectively for the hourly raw time series, reaching 0.77 and 0.63 after by applying a 30h running mean to filter out tides (Table 1). On the contrary, the meridional components (Figures 3b and 3f) show lower correlations, 0.27 for P1 and 0.29 for P3. These points are located in the AJ core, where the zonal velocity is one order of magnitude greater than the meridional component, so that the differences in the latter have small affection in the current roses (Figure 3g). The distributions of magnitudes and directions of the current at P1 for HFR and SAMPA are very close, with strong currents, that reach 2.5 m/s and point ENE mostly ($\sim$ 80%), the remaining heading East. At P3 the good agreement between HFR and SAMPA is maintained although currents are slightly weaker for the HFR, with maximum values between 1.5 and 2 m/s, while for SAMPA a small proportion of the measurements reach 2–2.5 m/s. In SAMPA the two prevailing directions at P3 are ESE ($\sim$ 30%) and E ($>$ 20%) while in the HFR the SE direction is also important at this location ($\sim$20%) and the E direction is less common ($<$ 10%).

At P2, located out of the AJ core, the two components of the velocity have the same magnitude and the effect of the discrepancies is noticeable. The correlation for the zonal components (Table 1 and Figure 3c) is lower than for the other two points: 0.41 for the raw hourly series and 0.52 for the low-passed series. For the meridional velocities (Table 1 and Figure 3d) the correlation is also low, with values similar to those of P1 and P3 (Table 1). Current roses show that for the HFR the prevailing directions vary between E and S while for SAMPA the current direction moves between E and N (Figure 3g).

The analysis of the time series shows that the agreement between HFR and SAMPA is better for the zonal than for the meridional component. In the AJ area, where the zonal velocities are higher, HFR and SAMPA coincide in both strength and direction of the current. On the other hand, in regions where the current is less zonal the discrepancies between radar and model are more noticeable and lower correlations for both components are obtained. The origin of these discrepancies is addressed in the following sections.

3.2. Mean Velocity Fields and Statistical Analysis

HFR and SAMPA monthly averaged velocity fields for months of February, May, August, and November, which illustrate the seasonal variability of the surface circulation in the Strait, are shown in Figure 4.The observed and modeled patterns match fairly well along the year, with maximum velocities found at the center of the Strait, reaching values around 1 m/s, and the magnitude and extension of the most energetic core of the AJ located in the same area in both systems. In February and November the AJ flows closer to the northern shore (Figures 4a, 4b, 4g, and 4h), shifting southward in the spring and summer months east of the Bay of Algeciras (Figures 4c–4f; the origin of this displacement will be discussed below). The main discrepancies are found at the northeastern boundary of the domain, an area affected by high GDOP in the meridional component (Figure 2b), which partly explains the differences between HFR and SAMPA observed in that region. Additionally, this zone of the domain is the furthest from the stations so the HFR

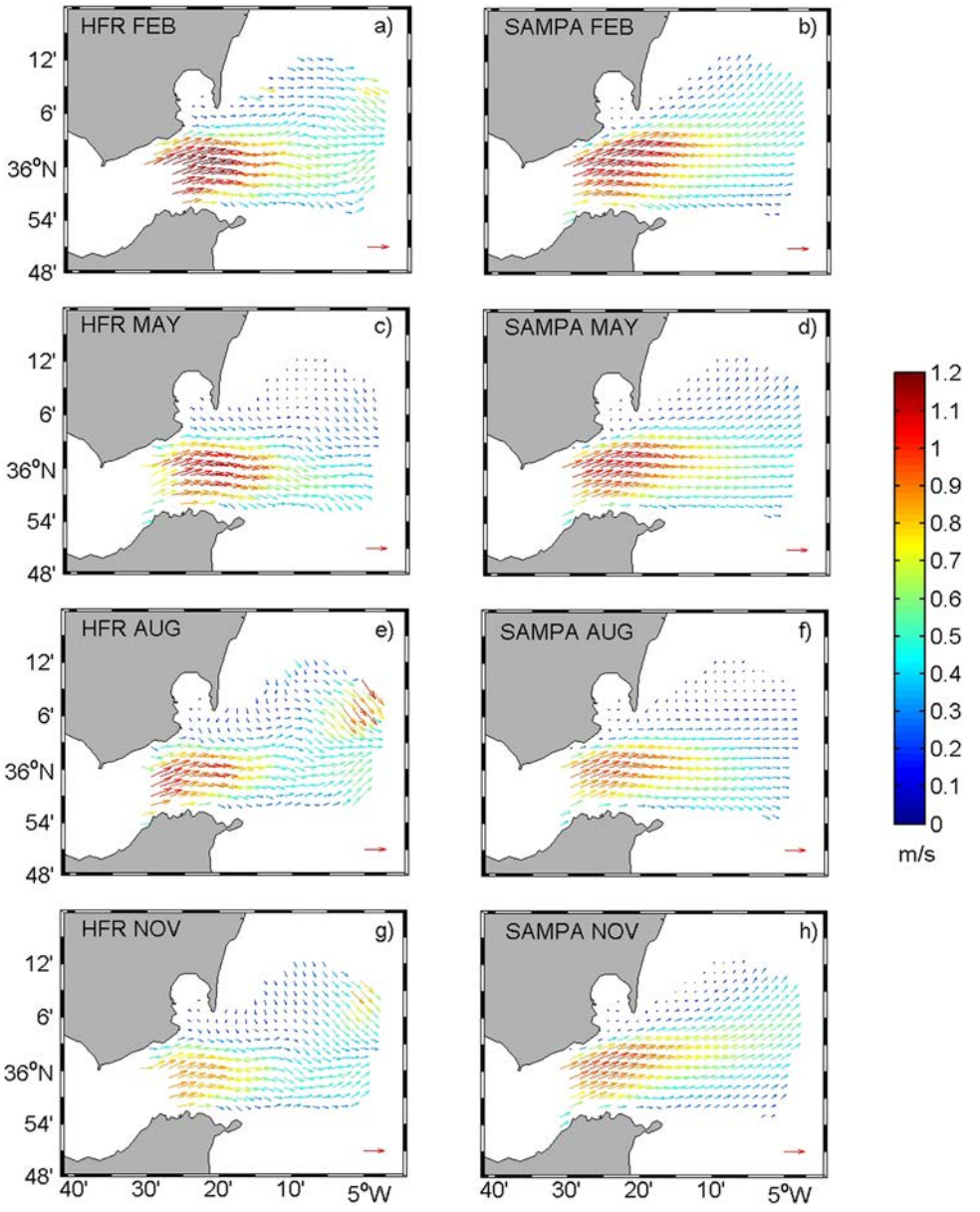

Figure 4. (a, b) February, (c, d) May, (e, f) August, and (g, h) November monthly mean velocity fields for (right) HFR and (left) SAMPA. The arrow in the lower right corner of each plot represents 1 m/s velocity.

back-scattered signal power is lower and more affected by the environmental distortion and hence a reduction in the data quality and time coverage are expected (Figure 1).

Although the AJ magnitude and direction are well reproduced by the model, the short spatial-scale variability of the current observed in the HFR field is not captured. While the flow describes several turnings east of the Bay of Algeciras in the HFR field, the direction of the jet only changes smoothly in SAMPA (Figure 4). Two reasons could explain this difference: the model wind forcing is based on 3 hourly outputs of 1/20° × 1/20° resolution (around 4.5 × 4.5 km), while radar data are hourly, with resolution of 1×1 km. As long as the wind forcing is more homogeneous in SAMPA and, therefore, it is unable to produce the short-scale meanders of the AJ observed by HFR. In addition, the fact that the surface level in SAMPA (2.5 m) is deeper than the level of HFR observations, which are representative of the first 0.5 m of the water column smoothes the effects of the wind stress on the stream direction. In other words, HFR observations, representative of a very thin surface layer, are more sensitive to the wind forcing.

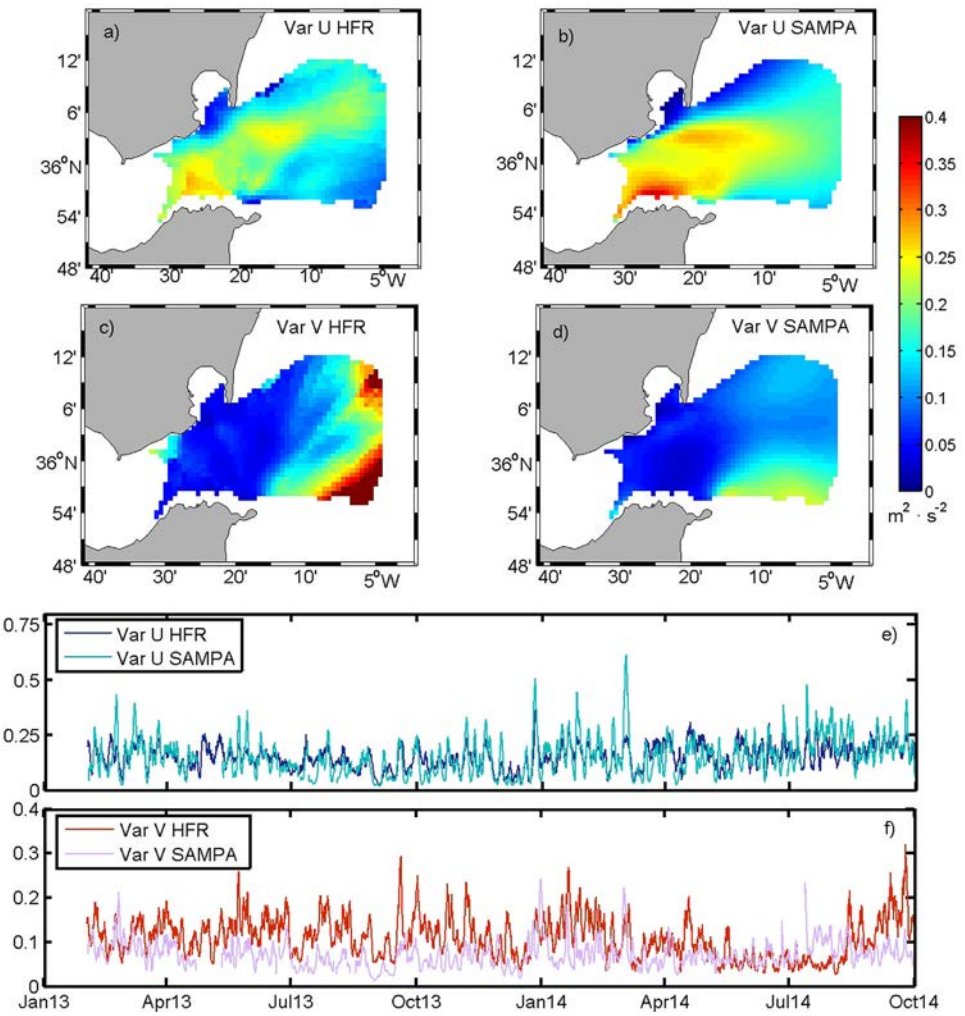

Figure 5. (a–d) Spatial distribution of the variance of zonal (U) and meridional (V) components of the HFR and SAMPA velocity fields. (e and f) show the time evolution of the spatially averaged variance of zonal (U) and meridional (V) components of the HFR and SAMPA velocity fields.

Similar considerations can be argued to explain the statistical differences observed in the comparison of the systems for the whole period (February 2013 to September 2014) summarized in Figures 5 and 6.The mean spatial distributions of the variance for the zonal and meridional velocities are very alike in both systems. The stronger variances are found in the zonal component, in the AJ path, where SAMPA shows slightly higher values (Figures 5a and 5b). Regarding the meridional component, the only remarkable difference is found at the eastern boundary of the domain, where HFR data are less reliable (Figures 5c and 5d). The time evolution of the spatially averaged variances of the zonal components is also very similar for HFR and SAMPA, with a correlation of 0.70, whereas it diminishes to 0.24 for the meridional component.

Regarding the statistical metrics, the complex correlation between the current vectors has a mean value of 0.38 for the whole domain (Figure 6a), reaching 0.60–0.75 in the area west of Ceuta that coincides with the strongest AJ velocities. The 75% of the veering angles are in the range [−15°, 15°], and only a small area in the southeastern corner present values higher than 20° (Figure 6b). The same pattern is observed for the correlation of the zonal component: higher values, reaching 0.8, in the AJ core and lower in the northwest (Figure 6c). However, for the meridional velocity the correlation is noticeably lower ($<$0.4), and even negative in some points (Figure 6d), as previously pointed out while analyzing the variance and the time series in section 3.1. The RMSE is again smaller in the areas of higher velocities, with values around 0.4 m/s for the zonal component (Figure 6e) and 0.2 m/s for the meridional (Figure 6f), increasing up to 0.9 m/s in the eastern boundaries of the domain.

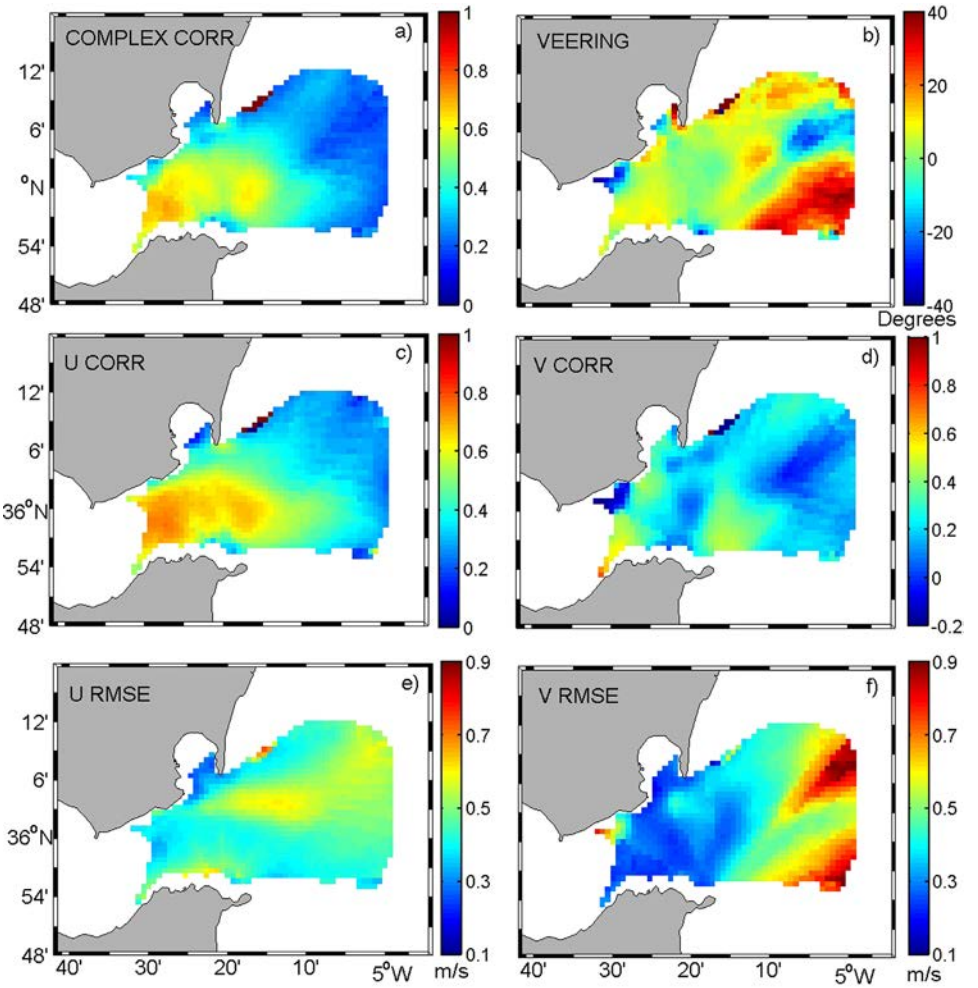

Figure 6. (a) Complex correlation between HFR and SAMPA vectors. (b) Veering angle between HFR and SAMPA vectors (measured counter-clockwise from the radar vector to the model vector). (c) Scalar correlation between the zonal velocity components. d) Scalar correlation between the meridional velocity components. e) Root mean square error between the zonal velocity components. (f) Root mean square error between the meridional velocity components. All metrics are estimated at 95% significance level.

Despite the poorer results in the outer domain, which are likely consequence of HFR technical limitations (GDOP and low data quality), previous works assessing model skills using HFR data show similar or lower values of correlation and higher RMSE (in relative terms) [*Cosoli et al*., 2013; O'*Donncha et al*., 2015]. The low correlation estimated for the meridional velocity in the AJ area is thought to be the result of the previously commented smoothed wind forcing in the model. The zonal current in this region is very strong, and its variability is largely conditioned by the mean and tidal exchanges, so it is less sensitive to the wind effects than the meridional component. Another point to be considered is that the main flow is almost perpendicular to the radial vectors of Punta Carnero and Ceuta sites, making the estimation of the HFR total vectors be less accurate [*Paduan et al*., 2006; *Robinson et al*., 2011].

3.3. Spectral Analysis and Tides

The average rotary power spectra of HFR and SAMPA, computed as described in section 2.4 to minimize the bias introduced by the short data gaps, are displayed in Figure 7. The concordance between both systems for the clockwise (CW) and counter-clockwise (CCW) components is high, especially in the band between semidiurnal and diurnal frequencies, where differences are lower than 20%. The M_2 CCW peak is more energetic, resulting in the predominance of cyclonically rotating ellipses (Figures 8a and 8c). The ellipses are highly eccentric in the westernmost area, where major axis amplitudes reach values of 45–50 cm/s for SAMPA, while for the HFR they are lower than 35 cm/s (Figures 8b and 8d). As we move eastward following

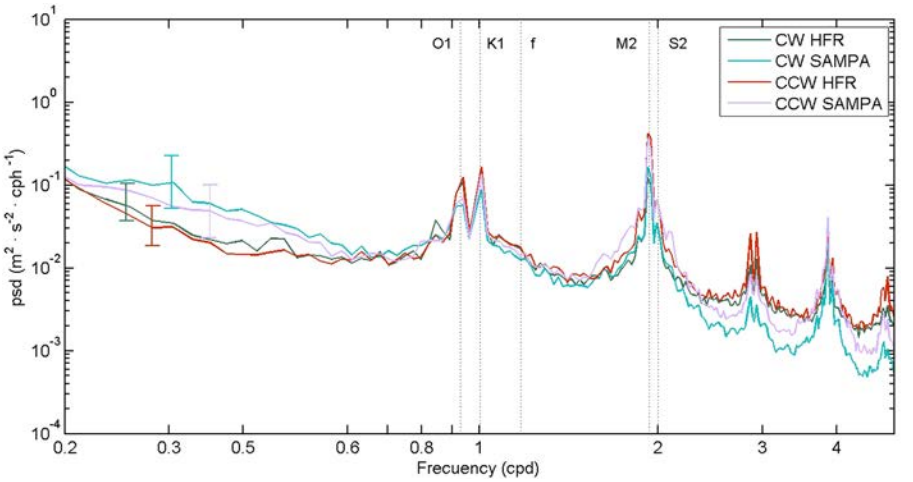

Figure 7. Spectral density of the rotary auto-spectra of HFR and SAMPA. Clockwise components are the green (HFR) and light blue (SAMPA) lines and counter-clockwise components are the red (HFR) and pink (SAMPA) lines. (f) Vertical lines indicate the frequencies of the semidiurnal (M_2, S_2) and diurnal (K_1, O_1) constituents, and the inertial oscillations. Vertical segments on the left indicate the frequency averaged 95% confidence intervals.

the AJ into the Alboran Sea, the ellipses become gradually less eccentric and their inclination turns clockwise. In the area east of the Bay of Algeciras, the HFR tidal currents are slightly stronger than SAMPA's ones, still the spatial distribution of the major axis amplitudes coincides in both systems except for a local maximum located in the southeastern corner of the domain, a spurious value consequence of the high meridional GDOP and low HFR coverage in that zone (Figures 1 and 2b). Quite probably, the ellipses orientations differ in the northeastern limit for the same reason. The same degree of agreement is obtained for the M_2 phase distribution (not shown). In the areas of the AJ and the Bay of Algeciras HFR and SAMPA phases are very similar, with differences lower than 15° that increase in the eastern areas of the domain.

For S_2, the CW and CCW components of the spectrum have similar intensity, leading to a combination of cyclonic and anti-cyclonic rotating ellipses (Figures 8e and 8g). As for M_2, amplitudes are larger in the western region for SAMPA (12–18 cm/s) than for HFR (∼10 cm/s), and the agreement is better east of the Bay of Algeciras where the amplitudes decay to 4–6 cm/s (Figures 8f and 8g). The eccentricity is also higher in SAMPA, and do not decrease eastward as for the HFR. In this case, the good agreement between HFR and SAMPA in the phase distribution is maintained practically over the whole domain. Small differences, of less than 10°, are found only in the easternmost areas (not shown).

The diurnal K_1 peaks for the CW and CCW components of the HFR spectrum are also comparable (Figure 7), and thus cyclonic and anti-cyclonic rotating ellipses are observed in figure 9a. For the model the CCW peak is slightly higher and the cyclonic rotation prevails (Figure 9c). A remarkable agreement is found for the inclination and eccentricity of HFR and SAMPA ellipses, particularly in the AJ area, where the inclination turns clockwise in the direction of advance of the jet in the same manner as the semidiurnal constituents do. The amplitudes are maxima in the southernmost strip (18–20 cm/s), decreasing eastward from Ceuta (Figures 9b and 9d). Large amplitudes (∼ 17 cm/s) are also found in the mouth of the Bay of Algeciras in SAMPA, and in the northeastern region of the domain in HFR. As for S_2, the phase distribution is almost the same for HFR and SAMPA in almost the whole domain, with very low differences (less than 15°) located in the northeastern areas (not shown).

The spatial distribution of the tidal ellipses, amplitudes and phases for O_1 replicates that of K_1. The HFR shows a wider area of clockwise rotating ellipses and stronger currents (Figures 9e and 9g). The energy in the CW and CCW peaks of the spectrum is lower in SAMPA, thus the amplitudes are also lower, with maximums values of 12 cm/s. The HFR reaches amplitudes of 20 cm/s in the area in front of the Ceuta site (Figures 9f and 9h). Again, high values are observed in the northeastern area, which are not reliable due to the high GDOP and low HFR coverage of that area.

The peaks in the high-frequency end of the spectra in Figure 7 correspond to the nonlineal constituents, which are caused by the strong topography-current interaction that happens in the Strait [*García-Lafuente*

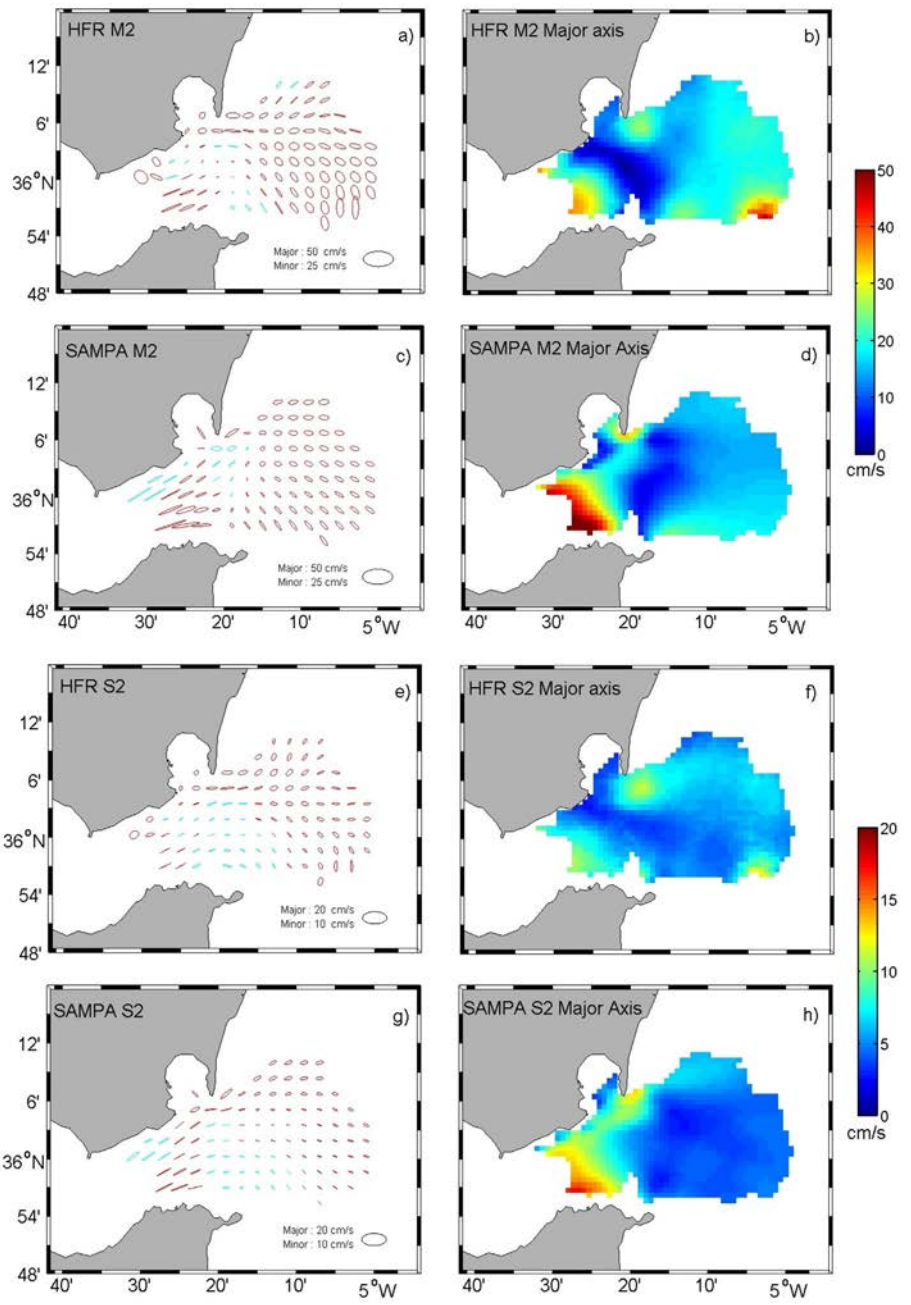

Figure 8. (left) Tidal ellipses and (right) amplitude of semimajor axes of semidiurnal (a–d) M_2 and (e–h) S_2 constituents. Blue (red) color of the ellipses in left plots indicates clockwise (counter-clockwise) rotation.

et al., 2000; *Baschek et al*., 2001; *Sánchez-Garrido et al*., 2008]. It is worth noticing that both systems resolve these high frequency constituents, which appear to be somewhat more energetic in the HFR system.

The energy of the inertial currents in the Strait is negligible in comparison with the tidal currents (Figure 7), and can be ignored. The strong sheared flow in the Strait hampers the appearance of inertial oscillations, which are sensitive to the shear vorticity.

Sanchez-Román et al. [2009] describe the spatial tidal variability along the Strait by analyzing observations and model outputs. For the semidiurnal constituents, the topographic constrain compels an amplitude maximum at Camarinal sill (CS in Figure 1), that decreases toward the eastern and western exits of the Strait. For M_2 the amplitudes vary from 50 cm/s at Tarifa to 25 cm/s at the entrance of the Alboran Sea, while for S_2

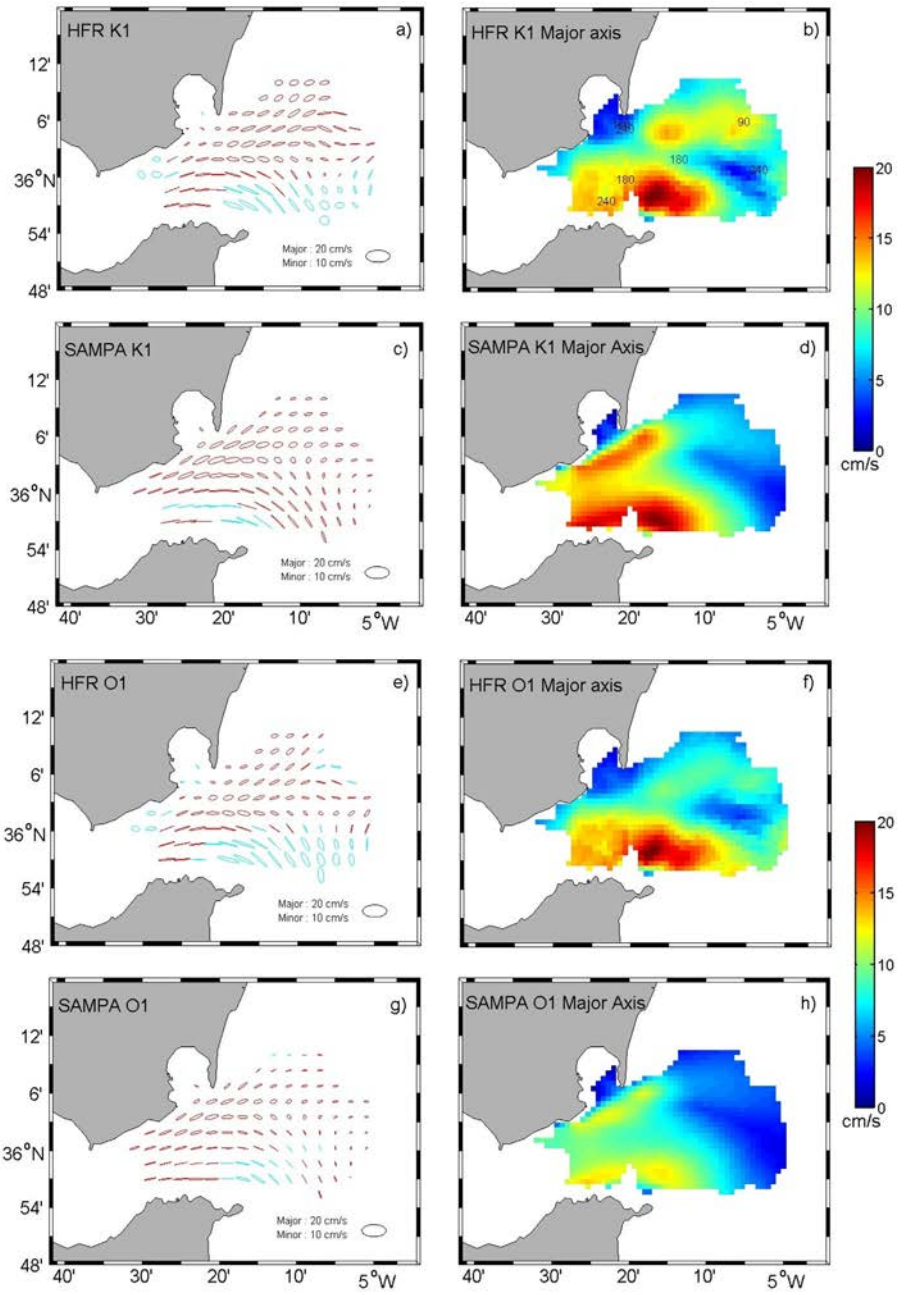

Figure 9. Same as Figure 7 except for the diurnal K_1 and O_1 constituents.

decrease from 15 to 20 cm/s to around 6 cm/s. The results of SAMPA are in better agreement in the westernmost region of the domain, where the HFR data quality is low because it coincides with the Tarifa-Ceuta baseline. In the rest of the domain SAMPA and HFR match the observations, with amplitudes decreasing to the west and showing similar values than those reported by *Sanchez-Román et al*. [2009].

For the diurnal constituents *Sanchez-Román et al*. [2009] found amplitude maxima of 18 cm/s around Tarifa for both K_1 and O_1, decreasing eastward to 10 cm/s nearby the Bay of Algeciras and to 5 cm/s in the easternmost areas of the HFR domain. Same values are observed in the radar and model for K_1, although the maxima displaced to the Ceuta site. For O_1 HFR matches the values of *Sanchez-Román et al*. [2009] better than SAMPA, whose amplitudes are slightly lower (Figure 9). Despite these differences, the magnitude and general pattern are consistent with the observations reported by *Sanchez-Román et al*. [2009].

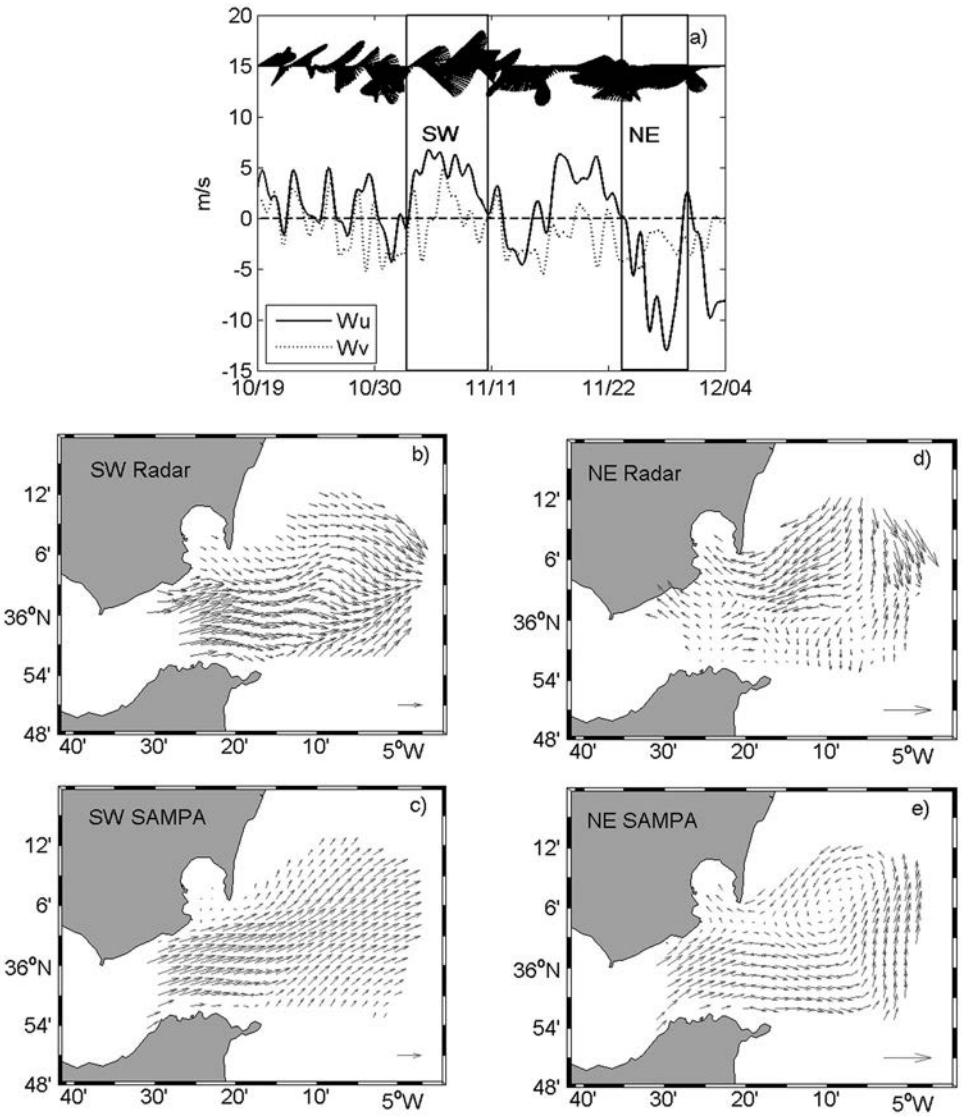

Figure 10. (a) Low-pass filtered wind record from the Punta Carnero buoy between October and December 2013. Solid (dotted) line is the zonal (meridional) component of the wind velocity. Sticks are oriented with respect to the north. The time-periods within rectangles are those selected for the analysis (see text). (b and c) The HFR and SAMPA mean velocity fields, respectively, during the westerlies period (5–9 November 2013), (d and e) The same during the easterlies period (26–30 November 2013). The arrows in the lower right corner of the plot indicate 1 m/s velocities (note that the scales are different for easterlies and westerlies).

3.4. Wind-Induced Circulation

In order to illustrate the response of HFR and SAMPA to the wind forcing on the surface circulation, episodes of the predominant winds in the area have been selected using data from buoy B1 (Figure 1). The mean velocity fields during two5 day periods of westerlies (5–9 November 2013) and easterlies (26–30 November 2013) are represented in Figure 8a.

Radar and model patterns during westerly winds (Figures 10b and 10c) are analogous to those of the mean circulation described in section 3.2 (Figure 4). The HFR field shows stronger currents and more variable direction in the AJ, pointing southward in a wide area of the northern region of the domain, from the Bay of Algeciras to the east. In SAMPA the velocity is rather homogeneous, pointing northeastward following the wind direction, except for the current flowing out of the Bay of Algeciras. As westerlies blow in the same direction of the AJ, their effects basically reinforce the current toward the Mediterranean and no significant modification with respect to the mean pattern is observed in HFR or SAMPA.

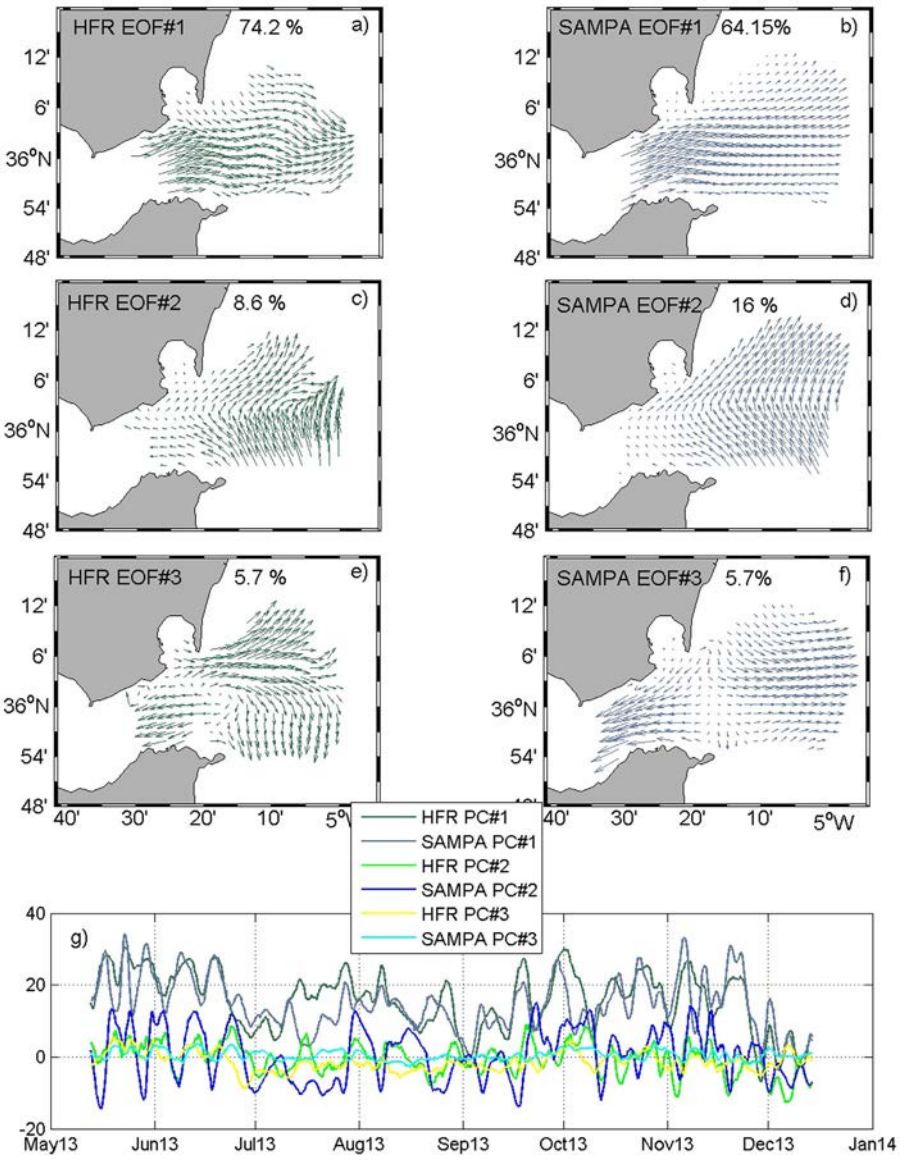

Figure 11. (a–f) Spatial patterns of the first EOF modes of (left) HFR and (right) SAMPA. The percent of variance explained by each mode is indicated on the plots. (g) Time series of the 30H running-mean of the principal components (PC) of each mode for HFR (PC#1 dark green, PC#2 light green and PC#3 yellow) and SAMPA (PC#1 dark blue, PC#2 blue and PC#3 light blue).

In the case of intense easterlies stronger differences are observed (Figures 10d and 10e). The HFR field shows an inversion of the flow in the surface layer over most of the domain, with a remarkable energetic counter-current in the Bay of Algeciras and northeastern areas. This counter-current, although weaker, is also present in the model, yet in the rest of the domain no inversion is observed. A cyclonic eddy, which does not appear in the HFR field, emerges at the northeast corner (Figures 10d and 10e) as a result of the combination of the mentioned southward counter-current and a northward flow in the easternmost boundary. In that region radar measurements are less accurate so the model field would be more realistic.

The potential of strong easterlies to reverse the flow has been previously reported and is not only limited to the surface. When combined with a rapid increase of the atmospheric pressure over the Mediterranean they can eventually reverse the entire Atlantic layer [*García-Lafuente et al.*, 2002c]. In the present case, the inversion is likely limited to the most superficial layer whose wind-induced circulation is much better captured by the radar due to the already pointed lower resolution of the model wind forcing and to the fact that its first z-level is 2.5 m.

Drawing the attention to the Bay of Algeciras area, results show that easterlies (westerlies) generate inflowing (outflowing) currents that are responsible for the vertical circulation and regulate the amount of Atlantic and Mediterranean waters present in the bay, as shown by *Sánchez-Garrido et al*. [2014]. These authors drew their conclusions from the SAMPA model whose wind-induced currents are weaker than those observed by the HFR system on the bay. It suggests that an enhanced renewal pattern could be obtained with a more realistic wind field capable of reproduce the HFR results in the surface layer.

The precision of the HFR systems describing the wind-induced circulation have been assessed in several works [*Cosoli et al*., 2007; *Gough et al*., 2010], and the better performance with respect to ocean models has been previously documented. O'*Donncha et al*. [2015] attribute the discrepancies they observed to model scale effects and to the parameterization of the wind stress coefficient, which is often estimated considering a constant winds peed over the domain. Here we assume that errors arise from the model wind forcing characteristics and configuration, yet further investigation is required to indentify and apply a better model parameterization.

3.5. EOF Decomposition

The results of the EOF decomposition applied to the raw hourly velocity fields are summarized in Figure 11. The first three modes account for the 87% and 86% of HFR and SAMPA variance, respectively. Only these modes are statistically significant according to the criterion suggested by *North et al*. [1982]. In general, both systems show satisfactory agreement for EOF#1 and EOF#2, while the agreement is less for EOF#3. The first mode has the same structure than the mean velocity field, as expected since the time average has not been removed from the original time series (Figures 11a and 11b). The correlation between the first principal components of SAMPA and HFR (PC#1, Figure 11g) reaches 0.65 after applying a 30 h running mean that removes the tidal variability. It highlights the agreement of model and radar describing the main flow pattern of the Strait.

The second mode captures the latitudinal shifting of the AJ mentioned in the analysis of the monthly mean flows in section 3.2. *Timmermans and Pratt* [2005] suggest that this shifting is a consequence of the hydraulic regime of the Strait, resulting from the interaction between current and topography. In particular, the detachment of the jet from the northern coast would take place when the exchanged flow switches from subcritical to supercritical. Although at monthly scale this phenomenon might be attenuated, it can be appreciated how during spring and summer months the AJ in the HFR and, especially in SAMPA, flows further south from the Spanish coast than in autumn or winter (Figure 4). These periods coincide with the maxima of the seasonal cycles of the outflow (April), and the inflow (August) when the possibility of attaining supercritical flows is higher [*García-Lafuente et al*., 2007; *Soto-Navarro et al*., 2010]. At shorter time scales, *Sánchez-Garrido et al*. [2014] found that this mechanism is relevant for the flushing times of the Bay of Algeciras, as it regulates the recirculation of the Atlantic water across its mouth. Here we show that the HFR system is also able to reproduce this process, even though it could be masked in the most superficial layer, where wind effects prevail. Indeed, HFR and SAMPA patterns are very similar (Figures 11c and 11d), and the correlation between the PC#2s is 0.58 (Figure 11g).

Lastly, EOF#3 reproduces the wind-induced circulation pattern (compare Figures 10d, 10e, and Figures 11e and 11f), for which the differences between HFR and SAMPA are higher. The spatial distributions do not match each other as they do for the first two modes and the correlation between PC#3s is very low (<0.1). This discrepancy would illustrate the limitations of the model to reproduce the short scale wind effect in the velocity field of the more superficial layer, which would be a consequence of the wind field configuration that forces the model, as it has been pointed out in previous sections. When comparing the zonal wind stress (τ_x) computed from the Punta Carnero buoy data with the PC#3 of model and radar, the better agreement with the latter is evident. The correlation between radar PC#3 and τ_x is 0.41 but it drops to 0.20 for the model. It should be noted that wind measurements have been collected in a single station located close to the coast (B1 in Figure 1), while the principal components are representative of the entire domain, thus the correlations are not expected to be very high.

4. Summary and Conclusions

This paper analyzes the surface circulation in the Strait of Gibraltar area provided by two operational systems during a 20 month period: a high frequency radar and high resolution ocean model. The velocity fields provided by both systems have been statistically compared, and their capacity to resolve the hydrodynamic processes of the area, such as the mean circulation, tides and wind-induced circulation, were assessed using different analysis methods.

The comparison of the velocity components at three different points distributed along the domain reveals a good agreement for the zonal components of the velocity of HFR and SAMPA, particularly in the AJ area, while larger differences are observed for the meridional components. The monthly mean patterns also show good agreement, with similar AJ strength and monthly variability. Higher discrepancies are found near the boundaries of the domain, where the accuracy of the HFR is lower. Apparently, the short scale variability of the AJ is better captured by the radar, which would be the result of the sparser resolution of the model wind forcing and also of the fact that the uppermost z-level of the model is 2.5 m, while HFR observations correspond to the 0.5 m thick superficial layer. The analysis of the variance and the statistical metrics reflect the previous results, with high vector and zonal correlations, and small veering angles and RMSE in a wide area of the domain. The higher differences are found in the meridional velocity, more sensitive to the wind forcing than the strong zonal component, which coincides with the direction of the incoming Atlantic Jet.

In the frequency range of tides, the radar and model concordance is even better, with spectral clockwise and counter-clockwise components almost coincident from the diurnal to semidiurnal band, which account for most of the tidal variability. The spatial distribution of M_2 and S_2 tidal ellipses is similar for model and radar in the AJ area, while some differences are observed in the north of the domain. Amplitudes in the model are larger and likely more realistic in the westernmost section, where the HFR data quality diminishes because this area is close to the Tarifa-Ceuta baseline. In the rest of the domain, east of the Bay of Algeciras, SAMPA model and HFR amplitudes are quite similar. For the diurnal constituents the differences are also small. Stronger currents and more CW rotating ellipses are observed for the radar, but the ellipses orientation and the amplitudes distribution go on showing a general good agreement, which even improves in the AJ area.

The analysis of the wind-induced circulation shows disagreement of the velocity field patterns provided by both systems, which we ascribe to the low spatial resolution of the wind-forcing field in the model and for the different depth of the uppermost cell, which is 2 m deeper in SAMPA. This is especially evident in the case of easterlies; HFR detects an inversion of the flow in the surface layer for a large part of the domain while in the model the inversion is limited to the counter-current of the Bay of Algeciras and Gibraltar areas.

The first three modes of the EOF decomposition explain around 85% of the variance of each data set, and capture the effect of the main sources of variability. The first mode corresponds to the mean field in both cases, which underlines the agreement of both systems in describing the general hydrodynamic features of the region. The second mode accounts for the latitudinal shifting of the AJ, which we have ascribed to changes of the hydraulic characteristics and the topographical constrains of the flow [*Timmermans and Pratt*, 2005; *Sánchez-Garrido et al*., 2014]. For these two leading modes, the spatial patterns of HFR and SAMPA are very close and the time coefficients are highly correlated. The third mode is representative of the local wind effect on the very superficial circulation. The discrepancies commented above are manifested here by the disparity of the spatial patterns and the very low correlation between their principal components. Notice however that their overall importance is limited since this mode only accounts for 5.7% of the variance of each data set.

The results summarized above reflect the capability of SAMPA model and the Gibraltar HFR system to properly describe the surface circulation of the Strait of Gibraltar area. The complementary character of model and radar has been put into relevance. Model data are more homogeneous in space and time so they complete the description of the HFR in the areas where the data quality or the time coverage are poorer. On the other hand, radar direct measurements are able to reveal model drawbacks and to incorporate subtle characteristics in the description of the most superficial circulation which is not well captured by the model, surely because of a deficient forcing wind field at the surface, which requires a better spatiotemporal resolution.

Acknowledgments
This work has been carried out in the frame of the CTM2012-33223 (OPERA) Ministerio de Economía y Competitividad Spanish-funded project. The HF radar system employed was installed in the frame of the European funded Transnational RADars for Environmental applications (TRADE) project. Partial support from CTM2013-40886-P project from the Spanish Ministerio de Economia y Competitividad is also acknowledged. Radar and model data are available through the website of Puertos del Estado (www.puertos.es).

References

Alfonso, M., E. Álvarez-Fanjul, and J. D. López (2006), Comparison of CODAR SeaSonde HF Radar operational waves and currents measurements with Puertos del Estado buoys, Final report, 1, pp. 1–32, Puertos del Estado, Spain.

Álvarez-Fanjul, E., B. Pérez-Gómez, and I. Rodríguez-Sánchez-Arévalo (2001), Nivmar: A storm surge forecasting system for Spanish waters, *Sci. Mar.*, *65*, 145–154.

Barrick, D. (2006), Geometrical Dilution of Statistical Accuracy (GDOSA) in Multi-Static HF Radar Networks, CODAR Ocean Sensors Ltd., Calif. [Available at http://www.codar.com/images/about/2006Barrick_GDOSA.pdf.]

Baschek, B., U. Send, J. García-Lafuente, and J. Candela (2001), Transport estimates in the Strait of Gibraltar with a tidal inverse model, *J. Geophys. Res.*, *106*, 31,033–31,044.

Bethoux, J. P., and B. Gentilli (1999), Functioning of the Mediterranean Sea: Past and Present Changes relaled to freshwater input and climatic changes, *J. Mar. Syst.*, *20*, 33–47.

Candela, J., C. D. Winant, and H. L. Bryden (1989), Meteorologically forced subinertial flows through the Strait of Gibraltar, *J. Geophys. Res.*, *94*, 12,667-12,679.

Carrere, L., and F. Lyard (2003), Modelling the barotropic response of the global ocean to atmospheric wind and pressure forcing – comparisons with observations, *Geophys. Res. Lett.*, *30*(6), 1–8.

Cats, G., and L. Wolters (1996), The Hirlam project, *International Journal of Computational Science and Engineering*, *3*, 4–7.

Chapman, R. D., L. K. Shay, H. C. Graber, J. B. Edson, A. Karachintsev, C. L. Trump, and D. B. Ross (1997), On the accuracy of HF radar surface current measurements: Intercomparison with ship-based sensors, *J. Geophys. Res.*, *102*, 18,737–18,748.

Chavanne, C., I. Janeković, P. Flament, P.-M. Pulain, M. Kizmić, and K.-W. Gurgel (2007), Tidal currents in the northwestern Adriatic: High-frequency radio observations and numerical model predictions, *J. Geophys. Res.*, *112*, C03S21, doi:10.1029/2006JC003523.

CODAR Ocean Sensors, Ltd. (2004), User's Information: About Baseline Interpolation, User Manual, Codar Ocean Sensors, Calif. [Available at http://www.codar.com/Manuals/Informative/Baseline_Interpolation.pdf.]

Cosoli, S., M. Gačić, and A. Mazzoldi (2007), Surface current variability and wind influence in the northeastern Adriatic Sea as observed from high-frequency (HF) radar measurements, *Cont. Shelf Res.*, *33*, 1–13.

Cosoli, S., A. Mazzoldi, and M. Gačić (2010),Validation of surface current measurements in the Northern Adriatic Sea from high-frequency radars, *J. Atmos. Oceanic Technol.*, *27*, 908–919.

Cosoli, S., M. Ličer, M. Vodopivec, and M. Malačič (2013), Surface circulation in the Gulf of Trieste (northern Adriatic Sea) from radar, model and ADCP comparisons, *J. Geophys. Res. Oceans*, *118*, 6138–6200, doi:10.1002/2013JC009261.

Criado-Aldeanueva, F., J. Soto-Navarro, and J. García-Lafuente (2012), Seasonal and interannual variability of surface heat and freshwater fluxes in the Mediterranean Sea: Budgets and exchange through the Strait of Gibraltar, *Int. J. Climatol.*, *32*, 286–302, doi:10.1002/joc.2268.

Crombie, D. D. (1955), Doppler spectrum of sea echo at 13.56 Mc/s, *Nature*, *175*, 681–682.

Dorman, C. E., R. C. Beardsley, and R. Limeburner (1995), Winds in the Strait of Gibraltar, *Q. J. R. Meteorol. Soc.*, *121*, 1903–1921.

Emery, B., M. L. Washburn, and J. A. Harlan (2004), Evaluating radial current measurements from CODAR high-frequency radars with moored current meters, *J. Atmos. Oceanic Technol.*, *21*, 1259–1271.

García-Lafuente, J., J. M. Vargas, F. Plaza, T. Sarhan, J. Candela, and B. Basheck (2000), Tide at the eastern section of the Strait of Gibraltar, *J. Geophys. Res.*, *105*, 14,197–14,213.

García-Lafuente, J., J. Delgado, J. M. Vargas, M. Vargas, F. Plaza, and T. Sarhan (2002a), Low-frequency variability of the exchanged flows through the Strait of Gibraltar during CANIGO, *Deep Sea Res., Part II*, *49*, 4051–4067.

García-Lafuente, J., E. Alvarez Fanjul, J. M. Vargas, and A. W. Ratsimandresy (2002b), Subinertial variability in the flow through the Strait of Gibraltar, *J. Geophys. Res.*, *107*(C10), 3168, doi:10.1029/2001JC001104.

García-Lafuente, J., J. Delgado, and F. Criado (2002c), Inflow interruption by meteorologoical forcing in the Strait of Gibraltar, *Geophys. Res. Lett.*, *29*(19), 1914, doi:10.1029/2002GL015446.

García-Lafuente, J., A. Sánchez-Román, G. Sannino, G. Diaz del Río, and J. C. Sanchez-Garrido (2007), Recent observations of seasonal variability of the Mediterranean outflow in the Strait of Gibraltar, *J. Geophys. Res.*, *112*, C10005, doi:10.1029/2006JC003992.

García-Lafuente, J., J. Delgado, A. Sánchez-Román, J. Soto, L. Carracedo, and G. Díaz del Río (2009), Interannual variability of the Mediterranean outflow observed in Espartel sill, western Strait of Gibraltar, *J. Geophys. Res.*, *114*, C10018, doi:10.1029/2009JC005496.

Gough, M. K., N. Gardfield, and E. McPhee-Shaw (2010), An analysis of HF radar measured surface currents to determine tidal, wind-forced, and seasonal circulation in the Gulf of Farallones, California, United States, *J. Geophys. Res.*, *115*, C04019, doi:10.1029/2009JC005644.

Graber, H. C., B. K. Haus, L. K. Shay, and R. D. Chapman (1997), HF radar comparisons with moored estimates of currents speed and direction: Expected differences and implications, *J. Geophys. Res.*, *102*, 18,749–18,766.

Kaihatu, J. M., R. A. Handler, G. O. Marmorino, and L. K. Shay (1998), Empirical orthogonal function analysis of ocean surface currents using complex and real-vector methods, *J. Atmos. Oceanic Technol.*, *15*, 927–941.

Kaplan, D. M., J. Largier, and L. W. Botsford (2005), HF radar observations of surface circulation off Bodega Bay (northern California, USA), *J. Geophys. Res.*, *110*, C10020, doi:10.1029/2005JC002959.

Kohut, J. T., and S. M. Glenn (2003), Improving HF radar surface current measurements with measured antenna beam patterns, *J. Atmos. Oceanic Technol.*, *20*, 1303–1316.

Kundu, P. K. (1976), Ekman Veering observed near the ocean bottom, *J. Phys. Oceanogr.*, *6*, 238–242.

Large, W. G., and S. Pond (1981), Open ocean momentum flux measurements in moderate to strong winds, *J. Phys. Oceanogr.*, *11*, 324–336.

Levanon, N. (2000), Lowest GDOP in 2-D scenarios, *IET Radar Sonar Navig.*, *147*(3), 149–155.

Lipa, B. J., and D. E. Barrick (1983), Least-squares method for the extraction of surface currents from CODAR Crossed-loop data: Application at ARSLOE, *IEEE J. Oceanic Eng.*, *8*, 226–253.

Lipa, B. J., B. Nyden, D. S. Ullman, and E. Terrill (2006), SeaSonde radial velocities: derivation and internal consistency, *IEEE J. Oceanic Eng.*, *31*, 850–861.

Lorente, P., J. Soto-Navarro, and E. Álvarez Fanjul (2014), Accuracy assessment of high frequency radar current measurements in the Strait of Gibraltar, *J. Oper. Oceanogr.*, *7*, 59–73.

Lorente, P., S. Piedracoba, and E. Alvarez Fanjul (2015), Validation of high-frequency radar ocean surface current observations in the NW of the Iberian Peninsula, *Cont. Shelf Res.*, *92*, 1–15.

Mariotti, A., M. V. Struglia, N. Zeng, and K.-M. Lau (2002), The hydrological cycle in the Mediterranean region and implications for the water budget of the Mediterranean Sea, *J. Clim.*, *15*, 1674–1690.

Marshall, J., C. Hill, L. Perelman, and A. Adcroft (1997), Hydrostatic, quasi-hydrostatic, and nonhydrostatic ocean modeling, *J. Geophys. Res.*,*102*(C3), 5733–5752.

Mau, J.-C-, D.-P. Wang, D. S. Ullman, and D. L. Codiga (2007), Comparison of observed (HF radar, ADCP) and model barotropic tidal currents in the New York Bight and Block Island Sound, *Estuarine Coastal Shelf Sci.*,*72*, 129–137.

Molcard, A., P. M. Poulain, P. Forget, A. Griffa, Y. Barbin, J. Gaggelli, J. C.De Maistre, and M. Rixen (2009), Comparison between VHF radar observations and data from drifter clusters in the Gulf of La Spezia (Mediterranean Sea), *J. Mar. Syst.*, *78*, S79–S89.

North, G. R., T. L. Bell, R. F. Cahalan, and F. J. Moeng (1982), Sampling errors in the estimation of empirical orthogonal functions, *Mon. Weather Rev.*, *110*, 699–706.

Oddo, P., M. Adani, N. Pinardi, C. Fratianni, M. Tonani, and D. Pettenuzzo (2009), A nested atlantic-mediterranean sea general circulation model for operational forecasting, *Ocean Science*, *5*, 461–473.

O'Donncha, F., M. Hartnett, S. Nash, L. Ren, and E. Ragnoli (2015), Characterizing observed circulation patterns within a bay using HF radar and numerical model simulations, *J. Mar. Syst.*, *142*, 96–110.

Ohlmann, C., P. White, L. Washburn, E. Terril, B. Emery and M. Otero (2007), Interpretation of coastal HF radar-derived currents with high-resolution drifter data, *J. Atmos. Oceanic Technol.*, *24*, 666–680.

Paduan, J. D., K. C. Kim, M. S. Cook, and F. P. Chávez (2006), Calibration and validation of direction-finding high-frequency radar ocean surface current observations, *IEEE J. Oceanic Eng.*, *31*(4), 862–875.

Pawlowicz, R., B. Beardsley, and S. Lentz (2002), Classical tidal harmonic analysis including error estimates in matlab using t_tide, *Comput. Geosci.*, *28*(8), 929–937.

Robinson, A. M., L. R. Wyatt, and M. J. Howarth (2011), A two year comparison between HF radar and ADCP current measurements in Liverpool Bay, *J. Oper. Oceanogr.*, *4*, 33–45.

Sammartino, S., J. García-Lafuente, J. C. Sánchez-Garrido, F. J. De los Santos, E. Álvarez-Fanjul, C. Naranjo-Rosa, M. Bruno, and C. Calero-Quesada (2014), A numerical model analysis of the tidal flows in the Bay of Algeciras, Strait of Gibraltar, *Continental Shelf Research*, *72*, 34–46, doi:10.1016/j.csr.2013.11.002.

Sánchez-Garrido, J. C., J. García Lafuente, F. Criado-Aldeanueva, A. Baquerizo, and G. Sannino (2008),Time-spatial variability observed in velocity of propagation of the internal bore in the Strait of Gibraltar, *J. Geophys. Res.*, *113*, C07034, doi:10.1029/2007JC004624.

Sánchez-Garrido, J. C., J. García-Lafuente, E. Álvarez Fanjul, M. García Sotillo, and F. J. de los Santos (2013), What does cause the collapse of the Western Alboran Gyre? Results of an operational ocean model, *Prog. Oceanogr.*, *116*, 142–153.

Sánchez-Garrido, J. C., J. García.Lafuente, S. Sammartino, C. Naranjo, F. J. de los Sntos, and E. Álvarez-Fanjul (2014), Meteorologically-driven circulation and flushing times of the Bay of Algeciras, Strait of Gibraltar, *Mar. Pollut. Bull.*, *80*, 97–106.

Sanchez-Román, A., G. Sannino, J. García-Lafuente, A. Carillo, and F. Criado-Aldeanueva (2009), Transport estimates at the western section of the Strait of Gibraltar: A combined experimental and numerical modeling study, *J. Geophys. Res.*, *114*, C06002, doi:10.1029/2008JC005023.

Sánchez-Román, A., J., García-Lafuente, J. Delgado, J. C. Sánchez-Garrido, and C. Naranjo (2012), Spatial and temporal variability of tidal flow at the Strait of Gibraltar, *J. Mar. Syst.*, *98-99*, 9–17.

Shadden, S. C., F. Lekien, J. D. Paduan, F. P. Chavez, and J. E. Marsden (2009), The correlation between surface drifters and coherent structures based on high-frequency radar data in Monterey Bay, *Deep Sea Res., Part II*, *56*(3-5), 161–172.

Soto-Navarro, J., F. Criado-Aldeanueva, J. García-Lafuente, and A. Sánchez-Román (2010), Estimation of the Atlantic inflow through the Strait of Gibraltar from climatological and in situ data, *J. Geophys. Res.*, *115*, C10023, doi:10.1029/2010JC006302.

Timmermans, M.-L-, E. and L. Pratt (2005), Two-layer rotating exchange flow between two deep basins: Theory ans application to the Strait of Gibtaltar, *J. Phys. Oceanogr.*, *35*, 1568–1592.

Trujillo, D. A., F. J. Kelly, J. C. Perez, H. R. Riddles, and J. S. Bonner (2004), Accuracy of surface current velocity measurements obtained from HF radar in Corpus Christi Bay, Texas, *IEEE Trans. Geosci. Remote Sens.*, *2*, 1179–1182.

Welch, P. D. (1967), The use of fast Fourier transform for the estimation of power spectra: A method based on time averaging over short, modified periodograms, *IEEE Trans. Audio Electroacoust.*, *AU-15*, 70–73.